



Addressing a systematic bias in carbon dioxide flux measurements with the EC150 and the IRGASON open-path gas analyzers



M. Helbig^{a,*}, K. Wischnewski^a, G.H. Gosselin^a, S.C. Biraud^b, I. Bogoev^c, W.S. Chan^b, E.S. Euskirchen^d, A.J. Glenn^e, P.M. Marsh^f, W.L. Quinton^f, O. Sonnentag^a

^a Département de géographie, Université de Montréal & Centre d'Études Nordiques, 520 Chemin de la Côte Sainte-Catherine, Montréal, QC H2V 2B8, Canada

^b Lawrence Berkeley National Laboratory, Berkeley, CA, USA

^c Campbell Scientific, Logan, UT, USA

^d Institute of Arctic Biology, University of Alaska Fairbanks, Fairbanks, AK, USA

^e Brandon Research and Development Centre, Agriculture and Agri-Food Canada, Brandon, MB, Canada

^f Cold Regions Research Centre, Wilfrid Laurier University, Waterloo, ON, Canada

ARTICLE INFO

Article history:

Received 12 April 2016

Received in revised form 21 July 2016

Accepted 22 July 2016

Keywords:

Carbon dioxide fluxes

Eddy covariance

Open-path infrared gas analyzer

Systematic error

Sensible heat

Absorption

ABSTRACT

Across a global network of eddy covariance flux towers, two relatively new open-path infrared gas analyzers (IRGAs), the IRGASON and the EC150, are increasingly used to measure net carbon dioxide (CO_2) fluxes (F_{CO_2}). Differences in net CO_2 fluxes derived from open- and closed-path IRGAs in general remain poorly constrained. In particular, the performance of the IRGASON and the EC150 for measuring F_{CO_2} has not been characterized yet. These IRGAs measure CO_2 absorption, which is scaled with air temperature and pressure before converting it to instantaneous CO_2 density. This sensor-internal conversion is based on a slow-response thermistor air temperature measurement. Here, we test if the high-frequency temperature attenuation causes selectively systematic F_{CO_2} errors that scale with kinematic temperature fluxes. First, we examine the relationship between wintertime F_{CO_2} and kinematic temperature fluxes for eight northern ecosystems. Second, we investigate how residuals between F_{CO_2} and CO_2 fluxes from co-located closed-path IRGAs (F_{CO_2}) are related to kinematic temperature fluxes for three different ecosystem types (i.e., boreal forest, grassland, and irrigated cropland). We find that kinematic temperature fluxes, but not mean ambient air temperatures or CO_2 flux regime, consistently determine the absolute magnitude of F_{CO_2} errors. This selectively systematic bias causes the most pronounced relative F_{CO_2} errors to occur when “true” CO_2 fluxes are low and kinematic temperature fluxes are high (e.g., northern ecosystems during the winter). The smallest relative errors occur during periods with large “true” CO_2 fluxes and low kinematic temperature fluxes. To address this bias, we replace the slow-response air temperature in the absorption-to- CO_2 density conversion with a fast-response air temperature derived from sonic anemometer measurements. The use of the fast-response air temperature improves the agreement between half-hourly F_{CO_2} and F_{CO_2} for all open- versus closed-path IRGA comparisons. Additionally, cumulative F_{CO_2} and F_{CO_2} sums are more comparable as differences drop from 63%–13% to 20%–8%. The improved IRGASON and EC150 performance enhances the ability and confidence to synthesize flux measurements across multiple sites including these two relatively new IRGAs.

© 2016 Elsevier B.V. All rights reserved.

1. Introduction

Turbulent net carbon dioxide (CO_2) fluxes (F_{CO_2} ; $\mu\text{mol m}^{-2} \text{s}^{-1}$) are measured across a global network of eddy covariance flux towers (Balocchi, 2001). These F_{CO_2} measurements are widely used to characterize global patterns of net ecosystem CO_2 exchange (e.g.,

Law et al., 2002; Beer et al., 2010; Migliavacca et al., 2015), to better understand the mechanisms behind its two component fluxes, ecosystem respiration and gross primary productivity (e.g., Falge et al., 2002; Mahecha et al., 2010), and to evaluate the performance of atmospheric CO_2 inversion models (e.g., Chevallier et al., 2012), global remote sensing-based biophysical models and land surface schemes (e.g., Verma et al., 2014). At more regional scales, net ecosystem exchange responses to a changing climate and/or to land use practices are often investigated across environmental

* Corresponding author.

E-mail address: manuel.helbig@umontreal.ca (M. Helbig).

Table 1Northern ecosystems with wintertime turbulent net CO₂ flux measurements made with the IRGASON or the EC150.

	ecosystem	latitude	longitude	instrument	h _m [m]	study period
Interior Alaska, AK	thermokarst bog	64.7°N	148.3°W	EC150	3	2011–2012
	fen			EC150	2	2011–2012
Scotty Creek, NT	boreal forest	61.3°N	121.3°W	EC150	15	2013–2016
	thermokarst bog			EC150	2	2014–2016
Mer Bleue, ON	boreal bog	45.4°N	75.5°W	EC150	3	2012
	tundra	68.8°N	133.5°W	EC150	4	2013–2014
Havikpak Creek, NT	subarctic woodland	68.3°N	133.5°W	EC150	12	2013
South Tobacco Creek, MB	cropland	49.3°N	98.3°W	IRGASON	2	2014–2015

gradients and across differing ecosystems (e.g., Litvak et al., 2003; Euskirchen et al., 2014; Knox et al., 2015).

To derive F_{CO_2} , high-frequency vertical wind velocity (w ; $m s^{-1}$) is measured with sonic anemometers and high-frequency atmospheric CO₂ (ρ_c ; $\mu\text{mol CO}_2 \text{ m}^{-2}$) and water vapor (ρ_v ; $\mu\text{mol H}_2\text{O m}^{-2}$) molar (mass) densities are measured with infrared gas analyzers (IRGA) (Baldocchi, 2008). Two broad IRGA types are generally used: open- and closed-path IRGAs. Closed-path IRGAs draw ambient air through an inlet tube and ρ_c and ρ_v are measured in an optical measurement cell. High-frequency air temperature (T_a ; K) fluctuations in the optical cell are attenuated in the intake tubing (e.g., Leuning and Judd, 1996; Aubinet et al., 2016). In contrast, open-path IRGAs measure ρ_c and ρ_v of the ambient air passing through the open-air sensing path. The sensing path is thus exposed to high-frequency T_a and ρ_v fluctuations.

Two relatively new open-path IRGAs, the IRGASON and the EC150 (Campbell Scientific Inc., Logan, UT, USA), are increasingly used for turbulent gas and energy flux measurements (e.g., Anderson and Wang, 2014; Euskirchen et al., 2014; Yuan et al., 2014; Semmens et al., 2015; Starkenburg et al., 2015; Ao et al., 2016; Chi et al., 2016; Helbig et al., 2016; Waldo et al., 2016). Their performance for measuring F_{CO_2} ($F_{c,OP}$; $\mu\text{mol CO}_2 \text{ m}^{-2} \text{ s}^{-1}$) has not been characterized yet, complicating their integration in synthesis studies across multiple sites. For another widely used open-path IRGA, the LI-7500 (LI-COR Biosciences, Lincoln, NE, USA), most studies report half-hourly differences of less than 5 % when compared to closed-path IRGAs (Anthoni et al., 2002; Ocheltree and Loescher, 2007; Wohlfahrt et al., 2008; Haslwanter et al., 2009; Bowling et al., 2010; Ueyama et al., 2012; Novick et al., 2013). In contrast, the few reported differences in the derived annual net ecosystem CO₂ exchange are poorly constrained and range from 1 % to 307 % with a mean difference of $89\% \pm 90\%$ (\pm one standard deviation; $n = 13$; Wohlfahrt et al., 2008; Burba et al., 2008; Haslwanter et al., 2009; Ueyama et al., 2012). By design, the EC150 is closely co-located with a modified CSAT3 sonic anemometer (CSAT3A, horizontal separation: 3 cm; Campbell Scientific, 2015a), whereas the IRGASON fully integrates the EC150 with the CSAT3A (horizontal separation: 0 cm; Campbell Scientific, 2015b). Thus, ρ_c , ρ_v , and w are measured at the same (IRGASON) or approximately at the same location (EC150). The flow distortion associated with the full integration of sonic anemometer and IRGA in the IRGASON causes small differences in vertical sonic temperature fluxes and velocity variance compared to a reference sonic anemometer (CSAT3; Horst et al., 2016), but also minimizes uncertainties due to sensor separation (Horst and Lenschow, 2009). Additionally, the co-location of sonic anemometer and IRGA allows deriving instantaneous CO₂ mixing ratios (χ_c ; mol mol⁻¹), a variable insensitive to T_a and ρ_v fluctuations (Kowalski and Serrano-Ortiz, 2007). However, high-frequency T_a and ρ_v fluctuations still influence the measured ρ_c (Webb et al., 1980) and affect the IRGA's direct measurement of CO₂ absorption through, for example, line broadening (Jamieson et al., 1963).

Absorption is the fraction of emitted light absorbed by the gas mixture along the IRGA's path length over a specific spectral range and is proportional to the number of molecules in the path.

To compensate for T_a and/or pressure effects on absorption line shape, absorption is scaled by gas temperature and/or pressure within the sensing path (Jamieson et al., 1963; Fratini et al., 2014). To convert the scaled absorption to ρ_c , a calibration function is derived for individual IRGASON and the EC150 units during factory calibration. The calibration function is derived through fitting measured absorption to known ρ_c and ρ_v across a wide range of pressure, infrared source temperature, and T_a (Campbell Scientific, 2015a; Campbell Scientific, 2015b). In contrast, T_a only marginally affects the broadband absorption measurements of the LI-7500. Air temperature is thus not included in its calibration function (e.g., Welles and McDermitt, 2005; Fratini et al., 2014). The use of a single absorption line of a tunable diode laser methane analyzer results in a pronounced instrument-specific T_a -sensitivity (i.e., spectroscopic effects; McDermitt et al., 2010). Similarly, the IRGASON's and the EC150's narrow infrared absorption bands might make them T_a -sensitive (Burch et al., 1962; Jamieson et al., 1963; Moore, 1983). Thus, to scale absorption with T_a , the IRGASON and the EC150 require instantaneous T_a measurements (Campbell Scientific, 2015a; Campbell Scientific, 2015b).

So far, the conversion of absorption to ρ_c has been based on T_a measured by a separate slow-response T_a thermistor probe ($T_{a,sf}$; K). Due to the thermal inertia of the probe and its radiation shield, $T_{a,sf}$ is not synchronized with the ρ_c measurements and is attenuated in the high-frequency range (Campbell Scientific, 2015b; Fig. S1). Consequently, when kinematic temperature flux ($w'\overline{T_a}$; m K s^{-1}) is positive, a fast ascending air parcel is warmer than indicated by $T_{a,sf}$, whereas a fast descending air parcel is colder (Webb et al., 1980). This T_a -bias propagates through the calibration function, ultimately causing a high-frequency ρ_c bias. This ρ_c bias is expected to correlate with T_a' (prime indicates deviation from the mean), which itself is correlated to w' when kinematic temperature flux unequal to 0 m K s^{-1} . As a consequence, errors in the raw CO₂ flux ($w'\overline{\rho_c}$; $\mu\text{mol CO}_2 \text{ m}^{-2} \text{ s}^{-1}$; overbar denotes the Reynolds average) are expected to scale with $w'\overline{T_a}'$. If the density fluctuation terms (sensible and latent heat flux within the measurement path; Webb et al., 1980) are measured accurately, $F_{c,OP}$ errors also scale with $w'\overline{T_a}'$ with. Hence, we expect $F_{c,OP}$ errors to vary with atmospheric conditions, that is, a selectively systematic bias (Moncrieff et al., 1996). We also expect that this bias can be eliminated or at least minimized by substituting $T_{a,sf}$ in the instantaneous CO₂ absorption-to- ρ_c conversion, with fast-response T_a ($T_{a,hf}$; K) measurements in the IRGA's open path. The fast-response T_a can be obtained from speed-of-sound measurements with the co-located sonic anemometer (Horst et al., 2016). Based on these theoretical considerations, the manufacturer of the IRGASON and the EC150 developed a beta version of the instrument's firmware that replaces $T_{a,sf}$ with $T_{a,hf}$ to convert absorption to ρ_c . Here, we characterize the performance of the IRGASON and the EC150 regarding $F_{c,OP}$ and compare $F_{c,OP}$ to $F_{c,CP}$. Using IRGASON and EC150 measurements, we test the hypotheses that (a) $F_{c,OP}$ errors scale with $w'\overline{T_a}'$ when $T_{a,sf}$ is used and that (b) using $T_{a,hf}$ to convert absorption to ρ_c minimizes this $F_{c,OP}$ bias. First, we analyze wintertime $F_{c,OP}$ obtained with the IRGASON and the EC150: we assume that the relative $F_{c,OP}$

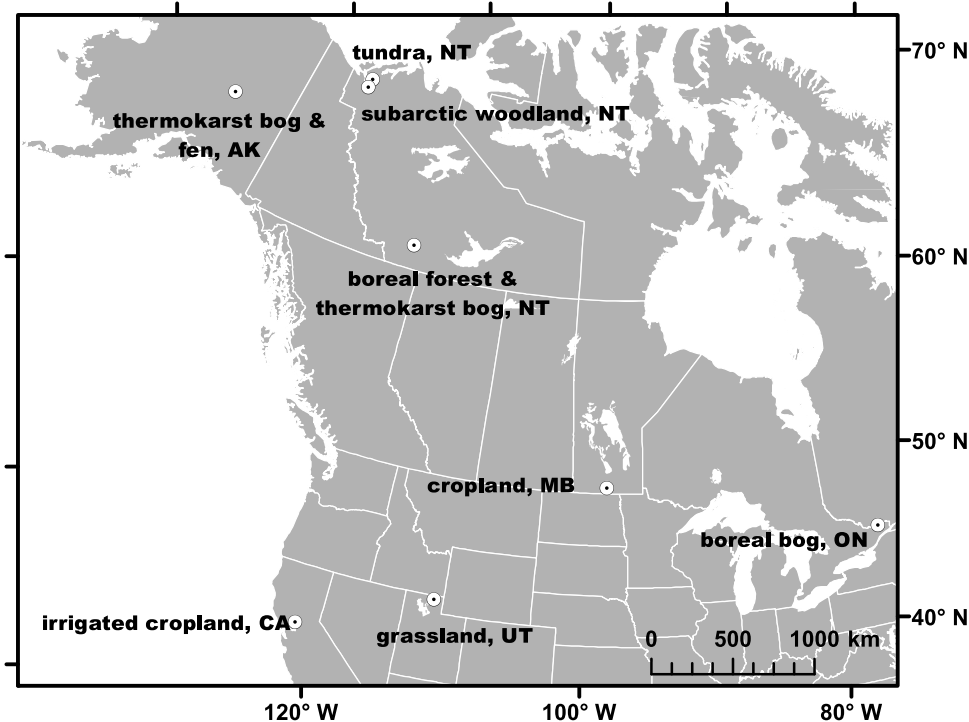


Fig. 1. Open- vs. closed-path IRGA comparisons were conducted at Scotty Creek, NT (boreal forest), at Logan, UT (grassland), and at Davis, CA (irrigated cropland). Wintertime CO₂ flux measurements using the IRGASON and the EC150 were conducted in interior Alaska (thermokarst bog & fen), at Trail Valley Creek, NT and Havikpak Creek, NT (tundra & subarctic woodland, respectively), at Scotty Creek, NT (boreal forest & thermokarst bog), at South Tobacco Creek, MB (cropland), and at the Mer Bleue bog, ON (boreal bog).

bias is most pronounced during periods when the “true” F_{CO_2} is very small (e.g., photosynthetic CO₂ uptake is unlikely and cold T_a limits ecosystem respiration), such as over northern ecosystems during the cold winter months (e.g., Lafleur et al., 2003; Goulden et al., 2006; Liu et al., 2006). We test if wintertime F_{c_OP} scale with w^*T_a across a range of northern (i.e., boreal, subarctic, and Arctic) ecosystems. Second, we compare open- vs. closed-path IRGAs: T_a fluctuations in closed-path IRGAs are attenuated, thus, w^*T_a -dependent errors in closed-path IRGA F_{CO_2} measurements (here EC155 [Campbell Scientific, Inc.] and LI-7200 [LI-COR Biosciences]; F_{c_CP} ; $\mu\text{mol m}^{-2} \text{s}^{-1}$) are assumed to be small. Using F_{c_CP} as a reference, we test if residuals between F_{c_OP} and F_{c_CP} (here defined as “ F_{c_OP} error”) scale with w^*T_a across four sensor comparisons from three flux tower sites. Third, we examine if the selectively systematic bias is minimized when the absorption conversion uses T_{a_hf} and evaluate how the resulting half-hourly and cumulative F_{c_OP} compare to F_{c_CP} .

2. Materials and methods

2.1. Study sites & instrumental setup

2.1.1. Wintertime F_{c_OP} measurements

Wintertime F_{c_OP} at eight northern ecosystems were defined as F_{c_OP} obtained when $T_a < -10^\circ\text{C}$. Measurements were conducted over a boreal forest and over a nearby thermokarst bog at Scotty Creek near Fort Simpson, NT (Helbig et al., 2016), at Mer Bleue, a bog near Ottawa, ON (Humphreys et al., 2014), at Havikpak Creek, a subarctic woodland, and at Trail Valley Creek, a shrub tundra site, both near Inuvik, NT (Eaton et al., 2001), over a thermokarst bog and a fen in interior Alaska (Euskirchen et al., 2014), and at South Tobacco Creek (Agriculture and Agri-Food Canada, 2013; <http://www.agr.gc.ca/eng/?id=1297269073820>), a cropland near Miami, MB (Fig. 1 & Table 1). To minimize the influence of “true” F_{CO_2} fluctuations

at the managed cropland, only late-winter F_{c_OP} in February were analyzed.

2.1.2. Scotty Creek, NT

Two sensor comparisons were conducted at Scotty Creek using two co-located open- and closed-path IRGAs (Table 2 & Fig. 1). Between 29 March and 10 April 2015 (“late winter”), an IRGASON was run concurrently with a LI-7200 using the same sonic anemometer (i.e., the IRGASON). An EC150 was run concurrently with the LI-7200 between 22 June and 16 August 2015 (“summer”) using the same CSAT3A (Table 2).

The IRGASON, the EC150, and the LI-7200 were mounted at ~ 15 m above the mean ground surface at the top of a tower structure. The length of the LI-7200 inlet tube was 0.35 m and the flow rate was set to 12 L min^{-1} . Ambient T_a at Scotty Creek (and at the other comparison sites) was measured with the EC150/IRGASON T_a probe, a 100K6A1B Thermistor (BetaTHERM Sensors, Galway, Ireland), and ambient pressure (P_a ; kPa) was measured with a PTB110 barometer (Vaisala, Helsinki, Finland).

The IRGASON and the LI-7200 were field-calibrated using the same zero (Ultra Zero Ambient Air, Praxair Canada Inc, Mississauga, ON, Canada) and 401-ppm CO₂ span gas ($\pm 1\%$; Praxair Canada Inc.) at the beginning and at the end of the late winter period. On 10 April 2015, the calibration check for the LI-7200 showed a zero-offset of 0.34 ppm and a span of 403.5 ppm (i.e., 0.5% drift in span). For the IRGASON, the zero offset was 1.9 ppm and the span was 407.2 ppm (i.e., 1% drift in span). At the end of the summer period, on 16 August 2016, the calibration check of the LI-7200 showed a zero offset of -9.3 ppm and a span of 393.9 ppm (i.e., 0.5% drift in span). For the IRGASON, the zero offset was 5.0 ppm and the span was 402.5 ppm (i.e., 0.9% drift in span).

Table 2

Instrumental setup for four studies comparing open- and closed-path eddy covariance (EC) systems using the IRGASON and the EC150 infrared gas analyzers (IRGA). For each study, measurement frequency (freq), horizontal and vertical distances ($dist_{hor}$ & $dist_{vert}$) between closed-path IRGA and sonic anemometer (sonic), measurement height of the EC systems (h_m), length of the study periods, and minimum and maximum air temperatures ($T_{a,min}$ & $T_{a,max}$) are listed.

	Open-path EC		Closed-path EC								
	IRGA	sonic	IRGA	sonic	freq [Hz]	dist _{hor} [cm]	dist _{vert} [cm]	h _{m,sonic} [m]	length [days]	T _{a,min} [°C]	T _{a,max} [°C]
Scotty Creek											
late winter	IRGASON	IRGASON	LI-7200	IRGASON	10	9	-12	15.2	13	-15	15
summer	EC150	CSAT3A	LI-7200	CSAT3A	10	10	-19	15.2	57	5	28
Logan	IRGASON	IRGASON	EC155	IRGASON	20	13.5	0	1.8	404	-20	37
Davis	IRGASON	IRGASON	EC155	CSAT3	10	15	-6	3.1	99	4	39

Table 3

Summary statistics of the relationships between wintertime turbulent net CO₂ flux measurements ($F_{c,OP}$; $\mu\text{mol m}^{-2} \text{s}^{-1}$) and kinematic temperature flux ($\overline{w'T_a'}$; m K s^{-1}), air temperature (T_a ; K), and half-hourly change in T_a (ΔT_a ; K).

$T_a < -10^\circ\text{C}$	$\overline{w'T_a'} - F_{c,OP}$						$T_a - F_{c,OP}$		$\Delta T_a - F_{c,OP}$	
	slope	95% CI	intercept	r ²	p-value	n	r ²	p-value	r ²	p-value
boreal forest, NT	-32.5	-33.6/-31.4	0.18	0.86	<0.001	1839	0.03	<0.001	0.20	<0.001
subarctic woodland, NT	-17	-18.5/-15.5	0.19	0.75	<0.001	164	0.05	0.004	0.01	0.21
cropland, MB	-16.7	-18.2/-15.4	0.28	0.34	<0.001	989	<0.01	0.31	0.02	<0.001
thermokarst bog, AK	-28.3	-30.2/-26.5	0.09	0.59	<0.001	623	0.01	0.003	<0.01	0.12
fen, AK	-43.9	-47.8/-40.7	0.19	0.65	<0.001	464	0.02	0.004	0.03	<0.001
boreal bog, ON	-31	-34.7/-28.7	0.34	0.76	<0.001	185	<0.01	0.37	0.05	0.003
tundra, NT	-47.7	-50.7/-44.8	0.09	0.86	<0.001	174	0.09	<0.001	0.04	0.008
thermokarst bog, NT	-33.6	-36.1/-31.2	0.17	0.60	<0.001	528	<0.01	0.83	0.09	<0.001

2.1.3. Logan, UT

Between 22 October 2014 and 30 November 2015, an IRGASON and an EC155 were deployed with a common sonic anemometer at a grassland site in Logan, UT (41.8°N , 111.9°W , Fig. 1 & Table 2). The EC155 intake tube was 58.4 cm long and the flow rate was set to 7 L min^{-1} . The EC155 was factory-calibrated by the manufacturer in June 2014 and the IRGASON in November 2011. Both IRGAs were zeroed with CO₂-free dry air on 20 August 2014 before the sensor comparison began.

2.1.4. Davis, CA

Between 07 April and 15 July 2015, an IRGASON and an EC155 with an independent CSAT3 were deployed over an irrigated cropland (alfalfa) in Davis, CA (38.5°N , 121.8°W , Fig. 1 & Table 2) as part of a larger gas analyzer experiment run by the AmeriFlux Management Project. The two eddy covariance systems were horizontally separated by 1.45 m. Both IRGAs were factory calibrated by Campbell Scientific, Inc., at the end of February 2015 and zeroed with CO₂-free dry air before the sensor comparison began. The daily automatic CO₂ zero (07 April to 15 July 2015) and span check (455.57 ppm span gas, 03 June to 15 July 2015) for the EC155 indicated minimal instrument drift with a mean zero-check of -0.7 ppm (range of -2.1 ppm to 1.8 ppm) and a mean span-check of 455.37 ppm (range of 453.05 ppm to 459.18 ppm , $<0.5\%$ drift in span).

2.2. Data handling and post-processing

To ensure site comparability, we applied the same flux processing for all comparison studies. We used the EddyPro software (version 6.1, LI-COR Biosciences) to derive half-hourly $F_{c,OP}$ and $F_{c,CP}$: negative $F_{c,OP}$ and $F_{c,CP}$ indicate a downward net CO₂ flux (i.e., toward the land surface), while positive $F_{c,OP}$ and $F_{c,CP}$ indicate an upward net CO₂ flux (i.e., toward the atmosphere). These turbulent fluxes were calculated using high-frequency measurements of w , $T_{a,hf}$, ρ_v , and ρ_c or χ_c . Vertical wind velocity and sonic temperature were derived from speed-of-sound measurements. Sonic temperature was converted to $T_{a,hf}$ by accounting for humidity effects (Schotanus et al., 1983). A double-rotation method was used to rotate the coordinate axes of the three-dimensional wind vec-

tor (McMillen, 1988) and a 30-min block-average was applied to extract turbulent fluctuations. Lag times between w and ρ_c and ρ_v (for $F_{c,OP}$), and χ_c and H₂O mixing ratios (for $F_{c,OP}$) were determined by covariance maximization using an automatic time lag optimisation procedure implemented in EddyPro.

For the closed-path IRGAs, we derived $F_{c,CP}$ as follows:

$$F_{c,CP} = \overline{\rho_d w' \chi_c'}, \quad (1)$$

where ρ_d (mol m^{-3}) is the dry air density. Instantaneous χ_c were calculated from ρ_c using T_a , ρ_v , and P_a measured inside the measurement cell (Ibrom et al., 2007a; Nakai et al., 2011; Burba et al., 2012).

For the open-path IRGAs, density effects related to T_a and ρ_v fluctuations were removed by applying the Webb-Pearman-Leuning (WPL) term (Webb et al., 1980; Leuning, 2007):

$$F_{c,OP} = \underbrace{\overline{w' \rho_c'}}_{\text{Term A}} + \frac{\overline{\rho_c}}{\overline{\rho_d}} \left(\underbrace{\overline{w' \rho_v'}}_{\text{Term B}} + \overline{\rho_a} \underbrace{\overline{w'T_a'}}_{\text{Term C}} \right), \quad (2)$$

where ρ_a (mol m^{-3}) is the moist air density. Term A is the raw CO₂ flux, term B is the H₂O dilution term related to the latent heat flux, and term C is the thermal expansion term related to the kinematic temperature flux. The kinematic temperature flux was corrected for humidity effects on sonic temperature following Dijk et al. (2004). An additional turbulent pressure flux term has been suggested to be negligible (Webb et al., 1980; Ono et al., 2008; Novick et al., 2013), unless the sites are characterized by frequent high winds and strong turbulence (e.g., $>10 \text{ m s}^{-1}$) (Massman and Lee, 2002). Here, no pressure flux term was used as mean wind speed was consistently below 10 m s^{-1} (Fig. S2).

We used closed-path IRGAs with short intake tubes (e.g., Leuning and Judd, 1996; Burba et al., 2012; Novick et al., 2013) and high tube flow rates (Massman and Ibrom, 2008) to minimize spectral attenuation. Spectral corrections for the closed-path IRGAs were applied according to Fratini et al. (2012). Additionally, we corrected for attenuation due to spatial separation between sonic anemometer and tube inlet (Horst and Lenschow, 2009). For the IRGASON and the EC150, spectral corrections according to

Moncrieff et al. (1997) were applied to all three covariance terms in Eq. (2) (Liu et al., 2006). The same high-pass filtering correction was applied for open- and closed-path systems (Moncrieff et al., 2004).

All analyses were restricted to stationary half-hours with well-developed turbulence and a good signal strength to limit lens contamination effects (Serrano-Ortiz et al., 2008) and to ensure high flux quality (Mauder and Foken, 2011). Remaining outliers were detected and discarded by the spike detection algorithm described by Papale et al. (2006) using a threshold value z of 4. All wind directions were accepted at Scotty Creek and Logan, where a common sonic anemometer was used. In this case, any flow distortion would similarly affect F_{c_OP} and F_{c_CP} . At Davis, several additional gas analyzers were mounted in close proximity of the two eddy covariance systems potentially distorting turbulent scalar fluxes (Wyngaard, 1981; Wyngaard, 1988). However, the F_{c_OP} - F_{c_CP} comparison results were independent of wind direction. Similarly, the comparison of the kinematic temperature fluxes derived from the two independent sonic anemometers did not vary with wind direction (Fig. S3). Thus, we did not apply any wind direction filter on F_{c_OP} or F_{c_CP} to maximize the sample size.

Wintertime F_{c_OP} at Scotty Creek, Havikpak Creek, Trail Valley Creek, South Tobacco Creek, and Mer Bleue were obtained as described above. Wintertime F_{c_OP} for the thermokarst bog and the fen sites in interior Alaska were obtained as described by Euskirchen et al. (2014).

2.3. Data analyses

To test if high-frequency T_a fluctuations bias wintertime F_{c_OP} and we used ordinary least-squares (OLS) regression between F_{c_OP} and the kinematic temperature flux $w'\overline{T_a}'$. We assumed that the “true” wintertime F_{CO2} was not correlated to $w'\overline{T_a}'$. To test if temperature-induced IRGA drifts might have affected wintertime F_{c_OP} , we applied OLS regression between F_{c_OP} and T_a and also between F_{c_OP} and half-hourly T_a changes (ΔT_a ; K). For all statistical analyses, we use a significance level of $\alpha = 0.05$. Confidence intervals (95% CI) of the regression slopes and offsets were derived using a bootstrapping approach by randomly sampling 1000 times the observed time series with replacement.

We compared F_{c_OP} with F_{c_CP} at Scotty Creek, Logan, and Davis using OLS regression and related summary statistics including the root mean square error (RMSE). Additional OLS regressions between F_{c_OP} - F_{c_CP} residuals and $w'\overline{T_a}'$ were applied to assess how $w'\overline{T_a}'$ affects the magnitude of the residuals, when T_{a_sf} is used for the open-path IRGA absorption conversion.

We expect errors in ρ_c (as measured by the IRGASON and the EC150) to increase with T_a' and in turn to cause increasing χ_c errors. In contrast, χ_c errors from closed-path IRGAs are expected to be independent of T_a' . Therefore, we assessed how high-frequency T_a fluctuations influence the ratio of high-frequency χ_c fluctuations derived from open- and closed-path IRGAs. First, we converted open-path IRGA ρ_c to χ_c . Then, we subtracted the 60 s-moving average of χ_c and T_a from the respective high-frequency time series and calculated the standard deviation for 1-min bins (σ_{T_a} and σ_{χ_c}). This procedure was applied to high-frequency time series for one day per site (08:00 h to 20:00 h). The time series were filtered for outliers according to Papale et al. (2006) to minimize outlier effects on σ_{T_a} and σ_{χ_c} . Finally, we calculated the ratio of σ_{χ_c} from open- and closed-path IRGAs ($\sigma_{\chi_{c_OP}}/\sigma_{\chi_{c_CP}}$).

To test how relative instrument drift (span and zero) between open- and closed-path IRGAs affects the comparison results, we calculated OLS regression statistics between outlier-filtered half-hourly open-path and closed-path IRGA $\overline{\rho_c}$. Closed-path IRGA $\overline{\rho_c}$ were derived by converting $\overline{\chi_c}$ using T_{a_sf} , P_a , and ρ_v from the open-path eddy covariance system. Subsequently, we applied the

Table 4

Summary statistics of the relationship between kinematic temperature fluxes ($w'\overline{T_a}'$) and residuals of turbulent net CO₂ fluxes (ΔF_{CO2}) measured by open-path (using a slow-response air temperature) and closed-path IRGAs.

	$w'\overline{T_a}' - \Delta F_{CO2}$		intercept	r^2	p-value	n
	slope	95% CI				
Scotty Creek boreal forest						
late winter	-14.9	-15.9/-14.1	0.08	0.82	<0.001	206
summer	-16.3	-16.9/-15.6	-0.08	0.76	<0.001	1316
Logan grassland	-14.2	-14.3/-14.0	0.05	0.91	<0.001	5206
Davis cropland	-16.0	-16.8/-15.2	-0.30	0.41	<0.001	2532

respective regression slopes to term A in Eq. (2) and applied intercept and slope to $\overline{\rho_c}$ in Eq. (2). Then, OLS regression statistics between the re-processed F_{c_OP} and F_{c_CP} and between their residuals and $w'\overline{T_a}'$ were recalculated.

To examine how using T_{a_hf} for the absorption conversion affects the F_{c_OP} - F_{c_CP} comparisons, CO₂ absorption data was collected for the IRGASON and the EC150 and converted to instantaneous ρ_c during post-processing. The conversion based on T_{a_hf} , as implemented in a beta version of the EC100 firmware, was performed with a MATLAB executable provided by the manufacturer. We compared the reprocessed F_{c_OP} (i.e., $F_{c_OP_hf}$) to F_{c_CP} using the same OLS regression approach as described above. We also calculated cumulative F_{c_OP} , $F_{c_OP_hf}$, and F_{c_CP} sums to assess the impact of replacing T_{a_sf} with T_{a_hf} on F_{c_OP} and F_{c_CP} integrals.

3. Results

3.1. Wintertime F_{c_OP} measurements with the IRGASON and the EC150

The relationships between $w'\overline{T_a}'$ and F_{c_OP} were significant across all northern ecosystems with a mean coefficient of determination (r^2) of 0.68 (Fig. 2 & Table 3). The slopes (intercepts) are negative (positive) and ranged from -43 to -16.7 $\mu\text{mol m}^{-2} \text{s}^{-1}$ per m K s^{-1} (0.09–0.34 $\mu\text{mol m}^{-2} \text{s}^{-1}$). At the forested ecosystems, wintertime F_{c_OP} ranged from -5.4 $\mu\text{mol m}^{-2} \text{s}^{-1}$ to 2.2 $\mu\text{mol m}^{-2} \text{s}^{-1}$ compared to only -1.4 $\mu\text{mol m}^{-2} \text{s}^{-1}$ to 2.7 $\mu\text{mol m}^{-2} \text{s}^{-1}$ for the non-forested ecosystems, with large negative F_{c_OP} being measured during periods when $w'\overline{T_a}'$ was positive (Fig. 2a).

Significant relationships between wintertime F_{c_OP} and T_a were only observed at five of the eight northern ecosystems (Table 3). Mean r^2 was 0.03 with a maximum r^2 of 0.09 for the tundra site. Similarly, ΔT_a was significantly correlated to wintertime F_{c_OP} at six northern ecosystems. Mean r^2 was 0.06 with a maximum r^2 of 0.20 at the boreal forest site.

3.2. F_{c_OP} vs. F_{c_CP} comparisons

The boreal forest at Scotty Creek, the grassland at Logan, and the irrigated cropland at Davis cover a wide range of F_{CO2} regimes. The smallest F_{c_CP} range was observed during the late winter at Scotty Creek with positive $F_{c_CP} < 1 \mu\text{mol m}^{-2} \text{s}^{-1}$. With a minimum F_{c_CP} of -41.7 $\mu\text{mol m}^{-2} \text{s}^{-1}$ and a maximum F_{c_CP} of 12.4 $\mu\text{mol m}^{-2} \text{s}^{-1}$, the largest F_{c_CP} range was observed at Davis (Fig. 3a-d).

Among the four comparisons, r^2 and slopes between F_{c_OP} and F_{c_CP} increased with the magnitude of F_{c_CP} (Fig. 3a-d). In contrast, F_{c_OP} - F_{c_CP} residuals showed a consistent negative relationship with $w'\overline{T_a}'$ with slopes of $\sim -15 \mu\text{mol m}^{-2} \text{s}^{-1}$ per m K s^{-1} (Fig. 3e-h & Table 4). Only weak relationships between T_a and F_{c_OP} - F_{c_CP} residuals were observed with r^2 ranging from 0.01 (Davis) to 0.17 (Scotty Creek, summer). Half-hourly T_a changes explained between 7% and 26% of the variance in the residuals. Correcting F_{c_OP} for the relative drift between open- and closed-path IRGAs resulted in sim-

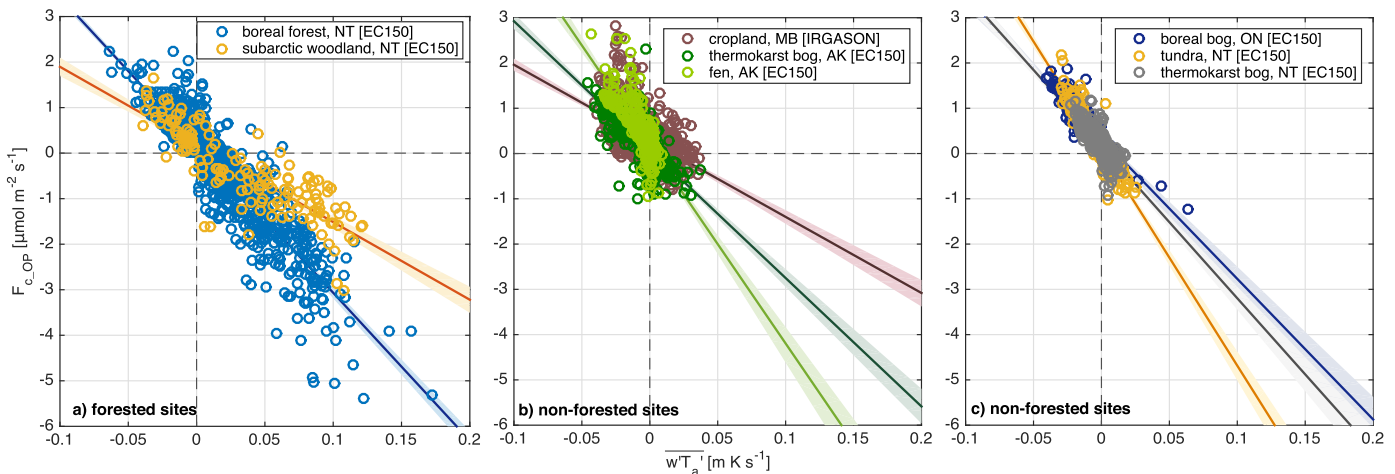


Fig. 2. Relationships between wintertime turbulent net CO₂ flux measurements by the IRGASON and the EC150 ($F_{c,OP}$) and kinematic temperature fluxes ($w'T_a$). Fluxes for forested sites (a) and non-forested (b & c) sites are shown separately due to their differing $w'T_a$ regimes. Solid lines indicate ordinary least-squares fits and shaded areas indicate 95% confidence intervals. All slopes are significant at $\alpha = 0.001$.

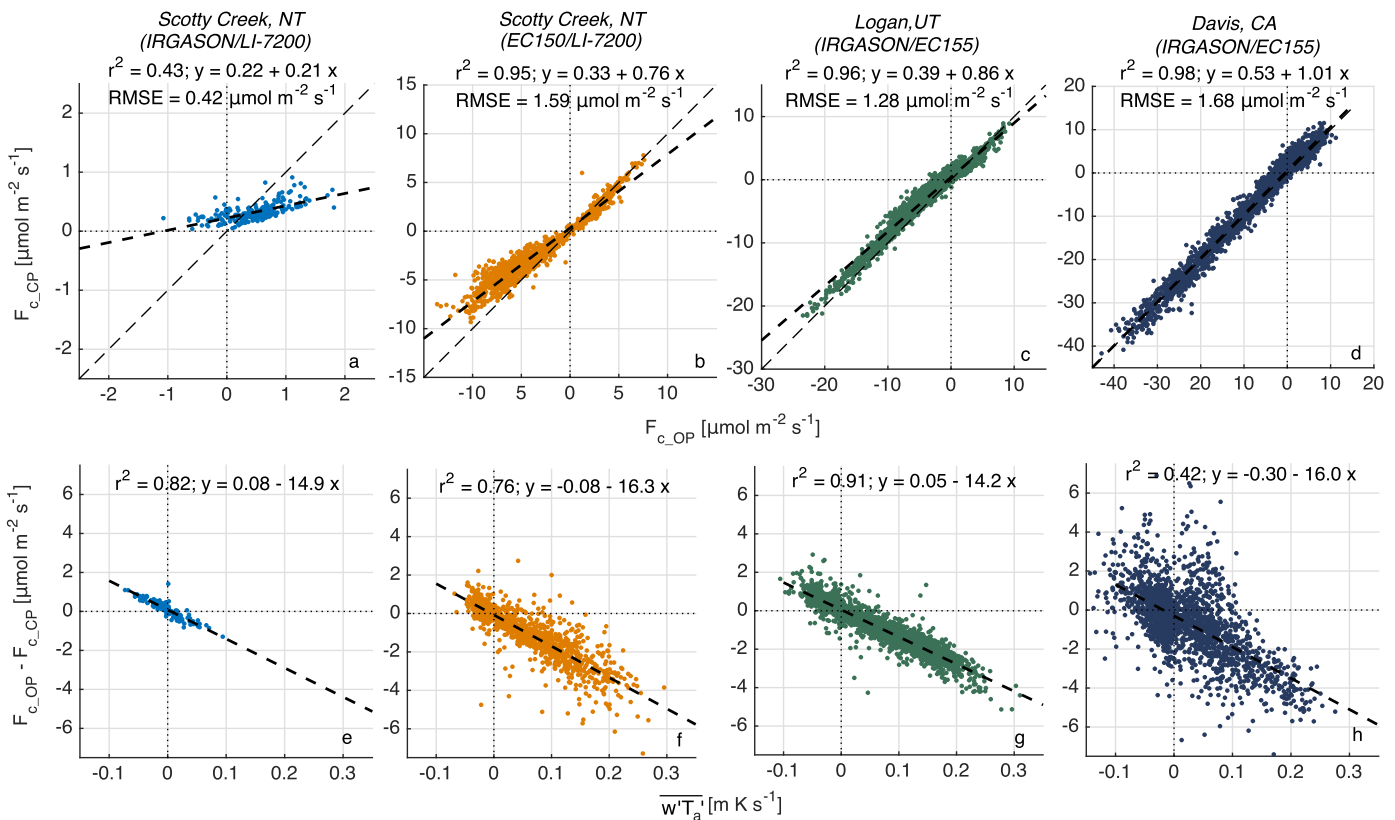


Fig. 3. (a-d) Comparison of turbulent net CO₂ fluxes measured by open-path ($F_{c,OP}$) and by closed-path IRGAs ($F_{c,CP}$) and (e-h) the relationship between their residuals with kinematic temperature fluxes ($w'T_a$) for four comparisons at three study sites. The respective open- and closed-path IRGAs deployed for each comparison are indicated above the figures. Dashed lines show ordinary least-squares fits. Note the different scales of the x- and y-axes for a-d.

ilar $F_{c,OP}$ - $F_{c,CP}$ differences and the negative relationships between their residuals and $w'T_a$ persisted (Fig. S4).

The ratio of high-frequency χ_c fluctuations, $\sigma\chi_{c,OP}/\sigma\chi_{c,CP}$, increased with increasing σT_a (Fig. 4). When σT_a were small (i.e., $\sigma T_a \approx 0^\circ\text{C}$), both IRGA types measured similar $\sigma\chi_c$ (i.e., the ratio is 1). The intercept for Logan and Davis was 0.99 compared to 1.07 and 1.32 at Scotty Creek during the late winter and the summer period, respectively. With increasing σT_a , the open-path IRGAs tended to overestimate $\sigma\chi_{c,OP}$ compared to closed-path IRGAs ($\sigma\chi_{c,CP}$).

indicating errors in the open-path IRGA's high-frequency ρ_c measurements.

3.2.1. Impact of a fast-response air temperature correction on $F_{c,OP}$

Re-processing instantaneous open-path IRGA ρ_c using $T_{a,hf}$ increased the r^2 between re-calculated $F_{c,OP}$ (i.e., $F_{c,OP,hf}$) and $F_{c,CP}$. At Davis, the slope of 1.01 did not change, while the slopes for the other sites increased by ≥ 0.1 . More importantly, the RMSE between

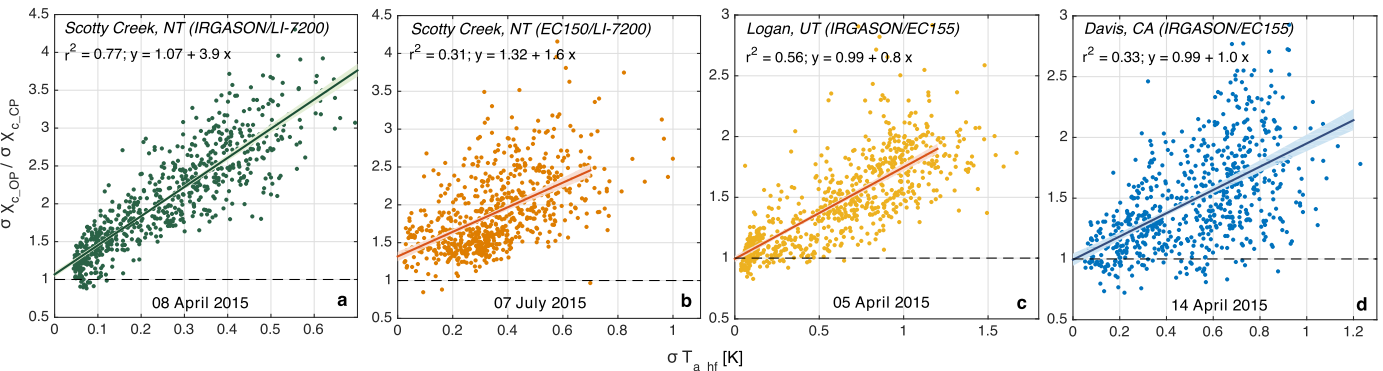


Fig. 4. Relationship between 1-min air temperature standard deviation (σT_a) and the ratio of 1-min mixing ratio standard deviation derived from open-path (OP) IRGAs ($\sigma \chi_{c,OP}$) and from the closed-path (CP) IRGAs ($\sigma \chi_{c,CP}$). Solid lines indicate ordinary least-squares fits and shaded areas indicate 95 % confidence intervals. Results are shown for one day per study site (between 08:00 and 20:00 local time).

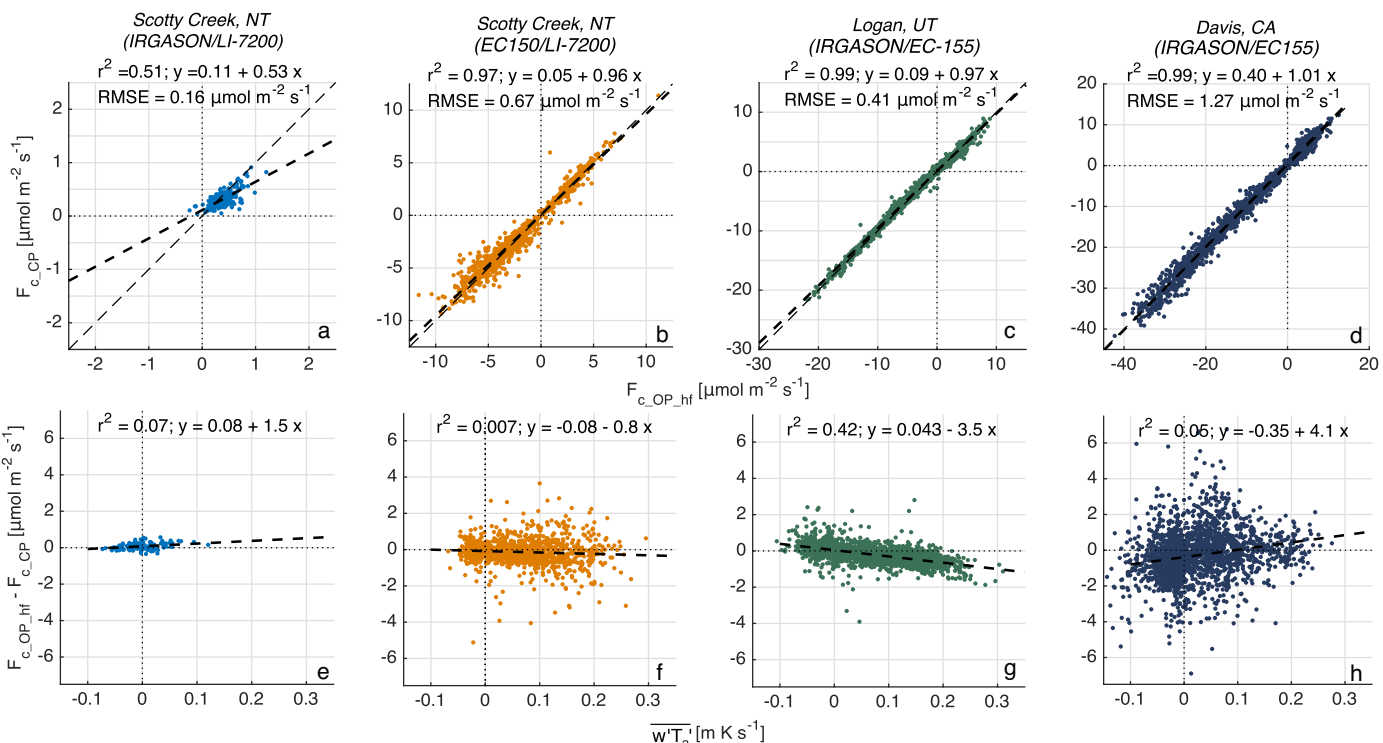


Fig. 5. Same as Fig. 3, but the absorption-to-CO₂ density conversion is based on a fast-response air temperature (derived from the sonic temperature, compared to a slow-response air temperature as used in previous versions of the EC100 firmware).

Table 5

Summary statistics of the relationship between kinematic temperature fluxes ($w' T_a'$) and residuals of turbulent net CO₂ fluxes measured by open-path (using a fast-response air temperature) and closed-path IRGAs ($\Delta F_{CO_2,hf}$).

$w' T_a' - \Delta F_{CO_2,hf}$						
	slope	95% CI	intercept	r^2	p-value	n
Scotty Creek boreal forest						
late winter	1.5	0.7/2.2	0.08	0.07	<0.001	206
summer	-0.8	-1.4/-0.2	-0.07	0.007	0.002	1324
Logan grassland	-3.5	-3.6/-3.4	0.04	0.42	<0.001	5191
Davis cropland	4.1	3.4/4.8	-0.39	0.05	<0.001	2607

$F_{c,OP}$ and $F_{c,CP}$ was reduced (Fig. 5a-d) and the kinematic temperature flux bias was minimized (Fig. 5e-h). When using $T_{a,hf}$, less than 10 % of the $F_{c,OP,hf} - F_{c,CP}$ variance (except for Logan) was explained by kinematic temperature fluxes (Fig. 5e-h & Table 5).

For all four comparisons, cumulative $F_{c,OP,hf}$ ($\Sigma F_{c,OP,hf}$; g CO₂ m⁻²) were more similar to $\Sigma F_{c,CP}$ compared to $\Sigma F_{c,OP} - \Sigma F_{c,CP}$ differences (Fig. 6). Relative $\Sigma F_{c,OP} - \Sigma F_{c,CP}$ differences ranged from 63 % (Fig. 6b) to 13 % (Fig. 6d). When using $T_{a,hf}$, these differences were reduced to 20 % for the late winter period at Scotty Creek (Fig. 6a) and to 8 % to 9 % for the other comparisons (Fig. 6b-d).

4. Discussion

4.1. Biased wintertime $F_{c,OP}$ measurements

Our analysis of wintertime $F_{c,OP}$ supports the hypothesis that $F_{c,OP}$ errors scale with $w' T_a'$ (Fig. 2). During periods with cold T_a , Burba et al. (2008) observed larger $F_{c,OP} - F_{c,CP}$ differences for the LI-7500 due to an unaccounted $w' T_a'$ increase within the open-path measurement path. This increase was attributed to an instrument surface heating effect. We observed only weak relationships

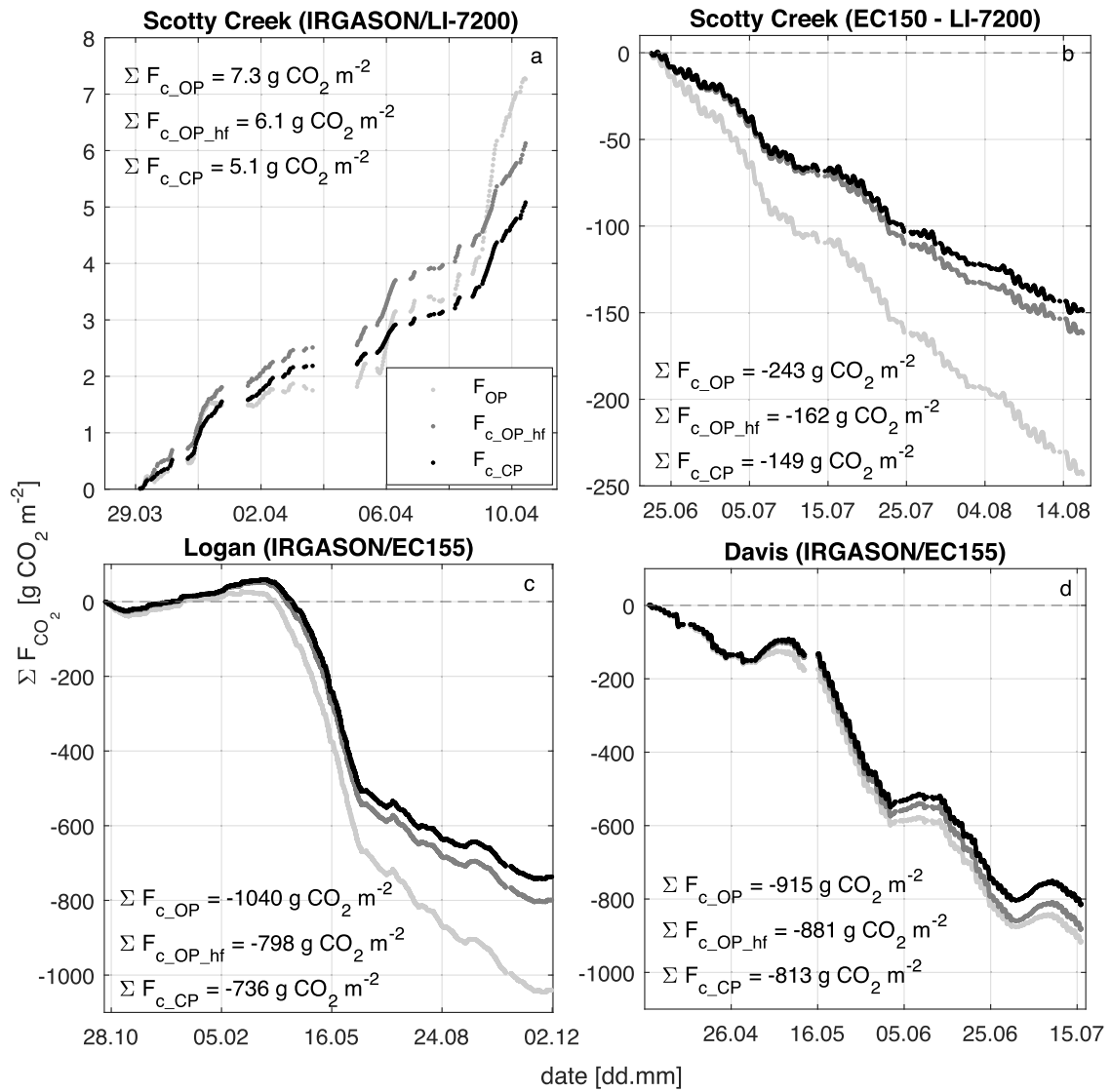


Fig. 6. Cumulative turbulent net CO_2 fluxes from closed-path IRGAs ($\Sigma F_{c,CP}$), from open-path IRGAs obtained using a slow-response air temperature to convert absorption measurements to CO_2 densities ($\Sigma F_{c,OP}$), and from open-path IRGAs obtained using a fast-response air temperature ($\Sigma F_{c,OP,hf}$). Only half-hours with high quality data for all systems were used and no gap-filling was applied.

between wintertime $F_{c,OP}$ and T_a (and ΔT_a) for the IRGASON and the EC150, suggesting that instrument surface heating is unlikely the reason for the observed negative wintertime $F_{c,OP}$ (Fig. 2). The IRGASON measures $w'T_a'$ in (or, for the EC150, very close to) the IRGA measurement path. Thus, the sonic anemometer would capture any additional heat flux in the measurement path, and the WPL term would adequately correct for the additional density fluctuations.

The $w'T_a'$ -dependence of wintertime $F_{c,OP}$ suggests that negative $F_{c,OP}$ are more likely observed at ecosystems with positive wintertime $w'T_a'$ (e.g., boreal forest; Betts et al., 1999; Launiainen et al., 2005; Amiro, 2010). In contrast, over snow-covered, low-stature vegetation with negative wintertime $w'T_a'$ (e.g., bogs, fens, tundra; e.g., Langer et al., 2011; Runkle et al., 2014; Knox et al., 2012) negative $F_{c,OP}$ measurements are less likely to be observed.

4.2. Selectively systematic errors in $F_{c,OP}$ obtained with the IRGASON and the EC150

Residuals of $F_{c,OP}$ and $F_{c,CP}$ consistently scaled with $w'T_a'$ (Fig. 3e-h & Table 4), providing evidence that $F_{c,OP}$ measurements

with the IRGASON and the EC150 are affected by selectively systematic errors. In contrast, relative $F_{c,OP}-F_{c,CP}$ differences decreased with an increasing $F_{c,CP}$ range (Fig. 3). At sites with large $F_{c,CP}$ magnitudes (e.g., croplands), the error-to-signal ratio is smaller compared to sites with small $F_{c,CP}$ (e.g., northern ecosystems in the winter). Such differences in $F_{c,CP}$ dynamics lead to a slope closer to unity at sites with large $F_{c,CP}$, even with the same absolute $F_{c,OP}$ errors (Fig. 3). When $F_{c,OP}-F_{c,CP}$ differences are caused by selectively systematic errors, then direct $F_{c,OP}-F_{c,CP}$ comparisons at sites with large $F_{c,CP}$ (Fig. 3 d) might mask the primary cause of these errors (e.g., errors scale with $w'T_a'$). In this case, the $F_{c,OP}-F_{c,CP}$ residuals are not necessarily proportional to $F_{c,CP}$. Instead, the residuals scale with a third, independent variable (e.g., $w'T_a'$) and an analysis of the residuals (Fig. 3e-h) is preferred over a direct comparison (Fig. 3a-d).

The relationship between $F_{c,OP}-F_{c,CP}$ residuals and $w'T_a'$ appears to be site- and instrument setup-independent. The slopes were similar ($\sim 15 \mu\text{mol m}^{-2} \text{ s}^{-1}$ per m K s^{-1}), despite the use of a common sonic anemometer for three comparisons (Scotty Creek and Logan) and of two spatially separated sonic anemometers for another comparison (Davis). The $w'T_a'$ from these two sonic anemometers

differed only slightly with a slope of 0.97 (Fig. S3), similar to the IRGASON's flow distortion effects on sensible heat fluxes reported by Horst et al. (2016). Thus, flow distortion appears not to cause the observed selectively systematic bias. The $F_{c,OP}$ bias also contrasts the good agreement between open- and closed-path IRGA latent heat fluxes (LE_{OP} and LE_{CP} ; Fig. S5, slopes between 0.97 and 1.08 for the four comparisons). The missing bias in LE_{OP} indicates that the $F_{c,OP}$ bias is unlikely to be related to uncertainties in spectral corrections. Spectral losses are small for $F_{c,OP}$ and LE_{OP} and usually more pronounced for LE_{CP} compared to $F_{c,CP}$ (e.g., Ibrom et al., 2007b; Fratini et al., 2012). Furthermore, the LE regime did not influence the relationship between $F_{c,OP}$ - $F_{c,CP}$ residuals and $w'T_a'$, as the slopes were not significantly different between comparisons with LE_{OP} ranges of -10 W m^{-2} to 40 W m^{-2} (Scotty Creek, late winter) and -10 W m^{-2} to 600 W m^{-2} (Davis; Fig. 3, Table 4 & Fig. S5). Therefore, water vapor effects on $F_{c,OP}$ or $F_{c,CP}$, either through density effects (Webb et al., 1980) or through spectroscopic cross sensitivities (e.g., Kondo et al., 2014), cannot explain the $F_{c,OP}$ bias.

The "IRGASON's" and the EC150's overestimation of $\sigma\chi_c$ with increasing σT_a (Fig. 4) suggests that using $T_{a,sf}$ (as implemented in the EC100 firmware), does not accurately compensate for the T_a -sensitivity of the absorption-to- ρ_c conversion in the high-frequency range. As a consequence, instantaneous ρ_c is biased and the bias persists in the χ_c calculation. The effects of the IRGAs' T_a -sensitivity on $F_{c,OP}$ are empirically demonstrated in this study. However, future research should investigate the exact physical causes of the instrument's T_a -sensitivity. For example, high-resolution transmission (HITRAN) simulations (Rothman et al., 2005) could be run to theoretically characterize this sensitivity.

Instrument drifts and calibration errors could cause small systematic $F_{c,CP}$ errors (e.g., Leuning and Judd, 1996; Fratini et al., 2014), but are likely negligible in this study, as demonstrated for Scotty Creek, where span drift was 1% or less for all IRGAs (IRGASON, EC150, LI-7200). Furthermore, during the first week of the comparisons, when instrument drift should be negligible, $F_{c,OP}$ - $F_{c,CP}$ residuals and $w'T_a'$ were significantly correlated (r^2 of 0.64, 0.82, 0.89, and 0.18 [$p < 0.001$] at Scotty Creek [late winter and summer], Logan, and Davis, respectively). Errors in corrections for spectral attenuation could also cause small systematic $F_{c,CP}$ errors (Aubinet et al., 2016). These errors would scale with the magnitude of $F_{c,CP}$ itself as the correction factor is directly applied to $w'\chi_c'$. As a result, $F_{c,CP}$ errors would be most pronounced during large negative $F_{c,CP}$, such as daytime measurements in the growing season (e.g., at Davis). During the winter, with small χ_c' and small (positive) $F_{c,CP}$, spectral correction errors would consequently have the least impact on $F_{c,CP}$ (e.g., during the winter at Scotty Creek).

To eliminate the influence of potential reference flux errors (e.g., $F_{c,CP}$), the IRGASON and the EC150 could be tested over a zero- CO_2 flux surface, such as a paved parking lot (Ham and Heilman, 2003). A parking lot experiment also minimizes water vapor fluxes. Small water vapor fluxes reduce $F_{c,OP}$ uncertainties due to water vapor cross-sensitivity (e.g., Leuning and Judd, 1996; Kondo et al., 2014). At the same time, large sensible heat fluxes allow assessing how using $T_{a,sf}$ affects the instantaneous absorption-to- ρ_c conversion. However, in this study, $F_{c,OP}$ - $F_{c,CP}$ residuals show a consistent relationship with $w'T_a'$ during both summer- and wintertime and across contrasting sites providing strong evidence that selectively systematic $F_{c,OP}$ errors scale with $w'T_a'$ and that this bias is mainly responsible for the $F_{c,OP}$ - $F_{c,CP}$ differences.

4.3. Improving $F_{c,OP}$ by using a fast-response air temperature to calculate CO_2 density

Replacing $T_{a,sf}$ with $T_{a,hf}$ for the absorption-to- ρ_c conversion resulted in a better agreement between $F_{c,OP}$ and $F_{c,CP}$ across all comparisons (Figs. 5 & 6). The conversion only affects instantaneous

ρ_c , and the WPL terms B (water vapor dilution) and C (temperature expansion, Eq. (2)) are not affected. Thus, selectively systematic $F_{c,OP}$ errors are mainly caused by errors in the raw CO_2 flux (WPL term A; Eq. (2); $w'p_c'$) while density effects (term B and C) are accurately captured. However, individual error sources generally cannot be singled out since multiple potential error sources (e.g., spectral correction, mean gas densities, temperature sensitivity, errors in CO_2 span) propagate through the WPL terms. These additional error sources can amplify or attenuate systematic $F_{c,OP}$ errors depending on the direction of individual errors (Liu et al., 2006). Together, such interacting error sources could explain the remaining small $F_{c,OP,hf}$ biases at Logan and Davis (Fig. 5g–h).

The use of $T_{a,hf}$ reduces the RMSE between $F_{c,OP}$ and $F_{c,CP}$ by more than 50 %, except for the Davis comparison where a larger scatter was observed (Figs. 3 d & 5 d). The larger scatter may be caused by the use of two separate sonic anemometers. Additionally, the two eddy covariance systems were separated by 1.45 m at a measurement height of 3.1 m. The separation may result in only partly overlapping flux footprints (e.g., Post et al., 2015).

At Davis, the largest absolute $F_{c,OP,hf}$ - $F_{c,CP}$ residuals of $>2 \mu\text{mol m}^{-2} \text{s}^{-1}$ were observed during periods with large, negative $F_{c,CP}$ (i.e., $F_{c,CP} < -20 \mu\text{mol m}^{-2} \text{s}^{-1}$). Using only half-hours when $F_{c,CP} > -20 \mu\text{mol m}^{-2} \text{s}^{-1}$ resulted in a stronger correlation between $F_{c,OP}$ - $F_{c,CP}$ residuals and $w'T_a'$ (r^2 increases from 0.42 [Fig. 3h] to 0.57 [Fig. S6c]) and the RMSE $F_{c,OP,hf}$ and $F_{c,CP}$ dropped from 1.27 (Fig. 5h) to 1.07 $\mu\text{mol m}^{-2} \text{s}^{-1}$ (Fig. S6b). During periods of large $F_{c,CP}$, larger spectral correction uncertainties (see above) and larger random $F_{c,CP}$ errors could explain this pattern (Richardson et al., 2006).

Using $T_{a,hf}$ also improved the agreement between $\Sigma F_{c,OP,hf}$ and $\Sigma F_{c,CP}$ compared to $\Sigma F_{c,OP}$ and $\Sigma F_{c,CP}$. For all sites with negative $\Sigma F_{c,CP}$, using $\Sigma F_{c,OP,hf}$ reduced the net CO_2 -sink strength estimate. This suggests that CO_2 -sink strengths are likely overestimated when using the IRGASON and the EC150 with $T_{a,sf}$ measurements. The largest relative improvement was observed for the summer period at Scotty Creek with relatively low $F_{c,CP}$. In contrast, $\Sigma F_{c,OP,hf}$ changed little (compared to $\Sigma F_{c,OP}$) for ecosystems with large $F_{c,CP}$, such as the irrigated cropland. Hirata et al. (2007) and Ueyama et al. (2012) used LI-7500 open-path IRGAs and co-located closed-path IRGAs (LI-6262 & LI-7000, LI-COR Biosciences) to quantify annual net ecosystem exchange rates of three temperate Larch forests and a rice paddy. Compared to the differences between $\Sigma F_{c,OP,hf}$ and $\Sigma F_{c,CP}$ (8 % to 20 %), they found larger differences in annual net ecosystem exchange rates between 60 % and 307 %. Compared to the multi-year differences in net ecosystem exchange rates reported by Haslwanter et al. (2009) for a temperate mountain grassland (4 % to 145 %; LI-7500 & LI-6262), the relative $\Sigma F_{c,OP,hf}$ - $\Sigma F_{c,CP}$ differences reported in this study are in the lower range.

In conclusion, we argue that studies using $F_{c,OP}$ measured with the IRGASON and the EC150 in conjunction with the slow-response T_a should treat these fluxes cautiously. When a fast-response T_a is used, the IRGASON and the EC150 performance for measuring $F_{c,OP}$ is comparable to the performance of closed-path IRGAs with short intake tubes. These constraints on differences between $F_{c,OP}$ and $F_{c,CP}$ improve the flux community's ability to use sites deploying the IRGASON and the EC150 for multi-site comparison and synthesis studies.

Acknowledgements

Given the theoretical considerations presented in this study and the observed wintertime $F_{c,OP}$ patterns, the IRGA manufacturer implemented an alternative sensor-internal method, using $T_{a,hf}$ in addition to $T_{a,sf}$, to derive ρ_c . This beta version of the EC100

control box firmware and the MATLAB executable to convert CO₂ absorption to CO₂ density are available on request from Campbell Scientific, Inc. The work at Scotty Creek was funded through the Canada Foundation for Innovation, the Canada Research Chairs Program, and a Natural Science and Engineering Council of Canada Discovery Grant to O.S. M.H. was funded through graduate student scholarships provided by the German Academic Exchange Service and the Fonds de recherche du Québec—Nature et technologies. We thank Wayne and Lynn McKay for logistical support as well as the Liidlii Kue First Nation and Dehcho First Nations in Fort Simpson, and the Jean-Marie River First Nation. We also thank the Government of the Northwest Territories (GNWT) for their support through the Wilfrid Laurier Laurier-GNWT Partnership Agreement. The intercomparison study at Davis, CA is supported by the Office of Biological and Environmental Research of the U.S. Department of Energy under contract No. DE-AC02-05CH11231 as part of the Terrestrial Ecosystem Science Program. Research at the Alaskan sites was funded by the U.S. Geological Survey Climate and Land Use Change Program, U.S. Geological Survey Climate Science Center, and the National Science Foundation. Research funding for the South Tobacco Creek site was provided to A.G. by the Agriculture and Agri-Food Canada Growing Forward 2 program and technical assistance by Clayton Jackson. We thank Elyn Humphreys (Carleton University), Gerardo Fratini & George G. Burba (LI-COR Biosciences), Meelis Mölder (Lund University), T. Andy Black (University of British Columbia), Janina Hommeltenberg (Karlsruhe Institute of Technology), Georg Wohlfahrt (University of Innsbruck), and Matteo Dettò (Smithsonian Tropical Research Institute) for valuable discussions on CO₂ gas analyzer comparisons. Finally, the anonymous reviewers are thanked for their contribution to improving the manuscript.

Appendix A. Supplementary data

Supplementary data associated with this article can be found, in the online version, at <http://dx.doi.org/10.1016/j.agrformet.2016.07.018>.

References

- Amiro, B., 2010. Estimating annual carbon dioxide eddy fluxes using open-path analysers for cold forest sites. *Agric. For. Meteorol.* 150, 1366–1372.
- Anderson, R.C., Wang, D., 2014. Energy budget closure observed in paired eddy covariance towers with increased and continuous daily turbulence. *Agric. For. Meteorol.* 184, 204–209.
- Anthoni, P.M., Unsworth, M.H., Law, B.E., Irvine, J., Baldocchi, D.D., Tuyl, S., Van Moore, D., 2002. Seasonal differences in carbon and water vapor exchange in young and old-growth ponderosa pine ecosystems. *Agric. For. Meteorol.* 111, 203–222.
- Ao, X., Grimmond, C.S.B., Chang, Y., Liu, D., Tang, Y., Hu, P., Wang, Y., Zou, J., Tan, J., 2016. Heat, water and carbon exchanges in the tall megacity of Shanghai: challenges and results. *Int. J. Climatol.*, <http://dx.doi.org/10.1002/joc.4657>.
- Aubinet, M., Joly, L., Loustau, D., De Ligne, A., Chopin, H., Cousin, J., Chauvin, N., Descarperiere, T., Gross, P., 2016. Dimensioning IRGA gas sampling systems: laboratory and field experiments. *Atmos. Meas. Tech.* 9, 1361–1367.
- Baldocchi, D.D., 2001. FLUXNET: a new tool to study the temporal and spatial variability of ecosystem-scale carbon dioxide, water vapor, and energy flux densities. *Bull. Am. Meteorol. Soc.* 82, 2415–2434.
- Baldocchi, D.D., 2008. Breathing of the terrestrial biosphere: lessons learned from a global network of carbon dioxide flux measurement systems. *Aust. J. Bot.* 56, 1–26.
- Beer, C., Reichstein, M., Tomelleri, E., Ciais, P., Jung, M., Carvalhais, N., Rödenbeck, C., Arain, M.A., Baldocchi, D., Bonan, G.B., Bondeau, A., Cescatti, A., Lasslop, G., Lindroth, A., Lomas, M., Luyssaert, S., Margolis, H., Oleson, K.W., Rouspard, O., Veenendaal, E., Viovy, N., Williams, C., Woodward, F.I., Papale, D., 2010. Terrestrial gross carbon dioxide uptake: global distribution and covariation with climate. *Science* 329, 834–838.
- Betts, A.K., Goulden, M.L., Wofsy, S.C., 1999. Controls on evaporation in a boreal spruce forest. *J. Clim.* 12, 1601–1618.
- Bowling, D.R., Marchetti, S.B., Lunch, C.K., Grote, E.E., Belnap, J., 2010. Carbon, water, and energy fluxes in a semiarid cold desert grassland during and following multiyear drought. *J. Geophys. Res.* 115, G04026.
- Burba, G.G., McDermitt, D.K., Grelle, A., Anderson, D.J., Xu, L., 2008. Addressing the influence of instrument surface heat exchange on the measurements of CO₂ flux from open-path gas analyzers. *Glob. Change Biol.* 14, 1854–1876.
- Burba, G.G., Schmidt, A., Scott, R.L., Nakai, T., Kathilankal, J., Fratini, G., Hanson, C., Law, B., McDermitt, D.K., Eckles, R., Furtaw, M., Velgersdyk, M., 2012. Calculating CO₂ and H₂O eddy covariance fluxes from an enclosed gas analyzer using an instantaneous mixing ratio. *Glob. Change Biol.* 18, 385–399.
- Burch, D.E., Gryvnak, D.A., Williams, D., 1962. Total absorptance of carbon dioxide in the infrared. *Appl. Optics* 1, 759–765.
- Campbell Scientific, 2015. EC150 CO₂ and H₂O Open-Path Gas Analyzer and EC100 Electronics with Optional CSAT3A 3D Sonic Anemometer. Logan, UT.
- Campbell Scientific, 2015. IRGASON Integrated CO₂/H₂O Open-Path Gas Analyzer and 3D Sonic Anemometer. Logan, UT.
- Chevallier, F., Wang, T., Ciais, P., Maignan, F., Bocquet, M., Altaf Arain, M., Cescatti, A., Chen, J., Dolman, A.J., Law, B.E., Margolis, H.A., Montagnani, L., Moors, E.J., 2012. What eddy-covariance measurements tell us about prior land flux errors in CO₂-flux inversion schemes. *Glob. Biogeochem. Cycles* 26, GB1021.
- Chi, J., Waldo, S., Pressley, S., O'Keeffe, P., Huggins, D., Stöckle, C., Pan, W.L., Brooks, E., Lamb, B., 2016. Assessing carbon and water dynamics of no-till and conventional tillage cropping systems in the inland Pacific Northwest US using the eddy covariance method. *Agric. For. Meteorol.* 218–219, 37–49.
- Dijk, A., Van Moene, A.F., de Bruin, H.A.R., 2004. The principles of surface flux physics: theory, practice and description of the ECPACK library, Internal Report 2004/1. Wageningen, Netherlands.
- Eaton, A.K., Rouse, W.R., Lafleur, P.M., Marsh, P., Blanken, P.D., 2001. Surface energy balance of the western and central Canadian Subarctic: variations in the energy balance among five major terrain types. *J. Clim.* 14, 3692–3703.
- Euskirchen, E.S., Edgar, C.W., Turetsky, M.R., Waldrop, M.P., Harden, J.W., 2014. Differential response of carbon fluxes to climate in three peatland ecosystems that vary in the presence and stability of permafrost. *J. Geophys. Res. Biogeosci.* 119, 1576–1595.
- Falge, E., Baldocchi, D.D., Tenhunen, J., Aubinet, M., Bakwin, P., Berbigier, P., Bernhofer, C., Burba, G., Clement, R., Davis, K.J., Elbers, J.A., Goldstein, A.H., Grelle, A., Granier, A., Gu, J., Hollinger, D., Kowalski, A.S., Katul, G., Law, B.E., Malhi, Y., Meyers, T., Monson, R.K., Munger, J.W., Oechel, W., Tha, K., Paw, U., Pilegaard, K., Rannik, Ü., Rebmann, C., Suyker, A., Valentini, R., Wilson, K., Wofsy, S., 2002. Seasonality of ecosystem respiration and gross primary production as derived from FLUXNET measurements. *Agric. For. Meteorol.* 113, 53–74.
- Fratini, G., Ibrom, A., Arriga, N., Burba, G., Papale, D., 2012. Relative humidity effects on water vapour fluxes measured with closed-path eddy-covariance systems with short sampling lines. *Agric. For. Meteorol.* 165, 53–63.
- Fratini, G., McDermitt, D.K., Papale, D., 2014. Eddy-covariance flux errors due to biases in gas concentration measurements: origins, quantification and correction. *Biogeosciences* 11, 1037–1051.
- Goulden, M.L., Winston, G.C., McMillan, A.M.S., Litvak, M.E., Read, E.L., Rocha, A.V., Rob Elliot, J., 2006. An eddy covariance mesonet to measure the effect of forest age on land-atmosphere exchange. *Glob. Chang. Biol.* 12, 2146–2162.
- Ham, J.M., Heilman, J.L., 2003. Experimental test of density and energy-balance corrections on carbon dioxide flux as measured using open-path eddy covariance. *Agron. J.* 95, 1393–1403.
- Haslwanter, A., Hammerle, A., Wohlfahrt, G., 2009. Open-path vs. closed-path eddy covariance measurements of the net ecosystem carbon dioxide and water vapour exchange: a long-term perspective. *Agric. For. Meteorol.* 149, 291–302.
- Helbig, M., Wischnewski, K., Kljun, N., Chasmer, L., Quinton, W.L., Dettò, M., Sonnentag, O., 2016. Regional atmospheric cooling and wetting effect of permafrost thaw-induced boreal forest loss. *Glob. Change Biol.*, <http://dx.doi.org/10.1111/gcb.13348>.
- Hirata, R., Hirano, T., Saigusa, N., Fujinuma, Y., Inukai, K., Kitamori, Y., Takahashi, Y., Yamamoto, S., 2007. Seasonal and interannual variations in carbon dioxide exchange of a temperate larch forest. *Agric. For. Meteorol.* 147, 110–124.
- Horst, T.W., Lenschow, D.H., 2009. Attenuation of scalar fluxes measured with spatially-displaced sensors. *Bound.-Layer Meteorol.* 130, 275–300.
- Horst, T.W., Vogt, R., Oncley, S.P., 2016. Measurements of flow distortion within the IRGASON Integrated Sonic Anemometer and CO₂/H₂O gas analyzer. *Bound.-Layer Meteorol.* 160, 1–15.
- Humphreys, E.R., Charron, C., Brown, M., Jones, R., 2014. Two bogs in the Canadian Hudson Bay Lowlands and a temperate bog reveal similar annual net ecosystem exchange of CO₂. *Arctic Antarct. Alp. Res.* 46, 103–113.
- Ibrom, A., Dellwik, E., Larsen, S.E., Pilegaard, K., 2007a. On the use of the Webb-Pearman-Leuning theory for closed-path eddy correlation measurements. *Tellus B* 59, 937–946.
- Ibrom, A., Dellwik, E., Flyvbjerg, H., Jensen, N.O., Pilegaard, K., 2007b. Strong low-pass filtering effects on water vapour flux measurements with closed-path eddy correlation systems. *Agric. For. Meteorol.* 147, 140–156.
- Jamieson, J.A., McFee, R.H., Plass, G.N., Gruber, R.H., Richards, R.G., 1963. *Infrared Physics and Engineering*. McGraw-Hill Company, Inc., New York, U.S.A.
- Knox, S.H., Carey, S.K., Humphreys, E.R., 2012. Snow surface energy exchanges and snowmelt in a shrub-covered bog in eastern Ontario, Canada. *Hydrol. Processes* 26, 1876–1890.
- Knox, S.H., Sturtevant, C., Matthes, J.H., Koteen, L., Verfaillie, J., Baldocchi, D., 2015. Agricultural peatland restoration: effects of land-use change on greenhouse gas (CO₂ and CH₄) fluxes in the Sacramento-San Joaquin Delta. *Glob. Change Biol.* 21, 750–765.
- Kondo, F., Ono, K., Mano, M., Miyata, A., Tsukamoto, O., 2014. Experimental evaluation of water vapour cross-sensitivity for accurate eddy covariance

- measurement of CO₂ flux using open-path CO₂/H₂O gas analysers. *Tellus B* 66, 23803.
- Kowalski, A.S., Serrano-Ortiz, P., 2007. On the relationship between the eddy covariance, the turbulent flux, and surface exchange for a trace gas such as CO₂. *Boundary-Layer Meteorol.* 124, 129–141.
- Lafleur, P.M., Roulet, N.T., Bubier, J.L., Frolking, S., Moore, T.R., 2003. Interannual variability in the peatland-atmosphere carbon dioxide exchange at an ombrotrophic bog. *Glob. Biogeochem. Cycles* 17, 1–14.
- Langer, M., Westermann, S., Muster, S., Piel, K., Boike, J., 2011. The surface energy balance of a polygonal tundra site in northern Siberia—Part 2. *Winter Cryosph.* 5, 509–524.
- Launiainen, S., Rinne, J., Pumpanen, J., Kulmala, L., Kolari, P., Keronen, P., Siivola, E., Pohja, T., Hari, P., Vesala, T., 2005. Eddy covariance measurements of CO₂ and sensible and latent heat fluxes during a full year in a boreal pine forest. *Boreal Environ. Res.* 10, 569–588.
- Law, B., Falge, E., Gu, L., Baldocchi, D., Bakwin, P., Berbigier, P., Davis, K., Dolman, A., Falk, M., Fuentes, J., Goldstein, A., Granier, A., Grelle, A., Hollinger, D., Janssens, I., Jarvis, P., Jensen, N., Katul, G., Mahli, Y., Matteucci, G., Meyers, T., Monson, R., Munger, W., Oechel, W., Olson, R., Pilegaard, K., Paw, U.K., Thorgeirsson, H., Valentini, R., Verma, S., Vesala, T., Wilson, K., Wofsy, S., 2002. Environmental controls over carbon dioxide and water vapor exchange of terrestrial vegetation. *Agric. For. Meteorol.* 113, 97–120.
- Leuning, R., 2007. The correct form of the Webb, Pearman and Leuning equation for eddy fluxes of trace gases in steady and non-steady state, horizontally homogeneous flows. *Boundary-Layer Meteorol.* 123, 263–267.
- Leuning, R., Judd, M.J., 1996. The relative merits of open- and closed-path analysers for measurement of eddy fluxes. *Glob. Change Biol.* 2, 241–253.
- Litvak, M., Miller, S., Wofsy, S.C., Goulden, M., 2003. Effect of stand age on whole ecosystem CO₂ exchange in the Canadian boreal forest. *J. Geophys. Res.* 108, 8225.
- Liu, H., Randerson, J.T., Lindfors, J., Massman, W.J., Foken, T., 2006. Consequences of incomplete surface energy balance closure for CO₂ fluxes from open-path CO₂/H₂O infrared gas analysers. *Bound.-Layer Meteorol.* 120, 65–85.
- Mahecha, M.D., Reichstein, M., Carvalhais, N., Lasslop, G., Lange, H., Seneviratne, S.I., Vargas, R., Ammann, C., Arain, M.A., Cescatti, A., Janssens, I.A., Migliavacca, M., Montagnani, L., Richardson, A.D., 2010. Global convergence in the temperature sensitivity of respiration at ecosystem level. *Science* 329, 838–840.
- Massman, W.J., Ibrom, A., 2008. Attenuation of concentration fluctuations of water vapor and other trace gases in turbulent tube flow. *Atmos. Chem. Phys.* 8, 6245–6259.
- Massman, W.J., Lee, X., 2002. Eddy covariance flux corrections and uncertainties in long-term studies of carbon and energy exchanges. *Agric. For. Meteorol.* 113, 121–144.
- Mauder, M., Foken, T., 2011. Documentation and Instruction Manual of the Eddy-Covariance Software Package TK3. Bayreuth, Germany.
- McDermitt, D., Burba, G., Xu, L., Anderson, T., Komissarov, A., Riensche, B., Schedlbauer, J., Starr, G., Zona, D., Oechel, W., Oberbauer, S., Hastings, S., 2010. A new low-power, open-path instrument for measuring methane flux by eddy covariance. *Appl. Phys. B* 102, 391–405.
- McMillen, R.T., 1988. An eddy correlation technique with extended applicability to non-simple terrain. *Bound.-Layer Meteorol.* 43, 231–245.
- Migliavacca, M., Reichstein, M., Richardson, A.D., Mahecha, M.D., Cremonese, E., Delpierre, N., Galvagno, M., Law, B.E., Wohlfahrt, G., Andrew Black, T., Carvalhais, N., Ceccherini, G., Chen, J., Gobron, N., Koffi, E., William Munger, J., Perez-Priego, O., Robustelli, M., Tomelleri, E., Cescatti, A., 2015. Influence of physiological phenology on the seasonal pattern of ecosystem respiration in deciduous forests. *Glob. Change Biol.* 21, 363–376.
- Moncrieff, J.B., Malhi, Y., Leuning, R., 1996. The propagation of errors in long-term measurements of land-atmosphere fluxes of carbon and water. *Glob. Change Biol.* 2, 231–240.
- Moncrieff, J.B., Massheder, J.M., de Bruin, H., Elbers, J., Friberg, T., Heusinkveld, B., Kabat, P., Scott, S., Soegaard, H., Verhoeft, A., 1997. A system to measure surface fluxes of momentum, sensible heat, water vapour and carbon dioxide. *J. Hydrol.* 188–189, 589–611.
- Moncrieff, J., Clement, R., Finnigan, J., Meyers, T., 2004. Averaging, detrending, and filtering of eddy covariance time series. In: Lee, X., Massman, W.J., Law, B. (Eds.), *Handbook of Micrometeorology*. Springer Netherlands, Amsterdam The Netherlands, pp. 7–31.
- Moore, C.J., 1983. On the calibration and temperature behaviour of single-beam infrared hygrometers. *Bound.-Layer Meteorol.* 25, 245–269.
- Novick, K.A., Walker, J., Chan, W.S., Schmidt, A., Sobek, C., Vose, J.M., 2013. Eddy covariance measurements with a new fast-response, enclosed-path analyzer: spectral characteristics and cross-system comparisons. *Agric. For. Meteorol.* 181, 17–32.
- Ocheltree, T.W., Loescher, H.W., 2007. Design of the AmeriFlux portable eddy covariance system and uncertainty analysis of carbon measurements. *J. Atmos. Ocean. Technol.* 24, 1389–1406.
- Ono, K., Miyata, A., Yamada, T., 2008. Apparent downward CO₂ flux observed with open-path eddy covariance over a non-vegetated surface. *Theor. Appl. Climatol.* 92, 195–208.
- Nakai, T., Iwata, H., Harazono, Y., 2011. Importance of mixing ratio for a long-term CO₂ flux measurement with a closed-path system. *Tellus* 63, 302–308.
- Papale, D., Reichstein, M., Aubinet, M., Canfora, E., Bernhofer, C., Kutsch, W., Longdoz, B., Rambal, S., Valentini, R., Vesala, T., Yakir, D., 2006. Towards a standardized processing of net ecosystem exchange measured with eddy covariance technique: algorithms and uncertainty estimation. *Biogeosciences* 3, 571–583.
- Post, H., Hendricks Franssen, H.J., Graf, A., Schmidt, M., Vereecken, H., 2015. Uncertainty analysis of eddy covariance CO₂ flux measurements for different EC tower distances using an extended two-tower approach. *Biogeosciences* 12, 1205–1221.
- Richardson, A.D., Hollinger, D.Y., Burba, G.G., Davis, K.J., Flanagan, L.B., Katul, G.G., Munger, J.W., Ricciuto, D.M., Stoy, P.C., Suyker, A.E., Verma, S.B., Wofsy, S.C., 2006. A multi-site analysis of random error in tower-based measurements of carbon and energy fluxes. *Agric. For. Meteorol.* 136, 1–18.
- Rothman, L.S., Gordon, I.E., Barbe, A., Benner, D.C., Bernath, P.F., Birk, M., Boudon, V., Brown, L.R., Campargue, A., Champion, J.P., Chance, K., Couder, L.H., Dana, V., Devi, V.M., Fally, S., Flaud, J.M., Gamache, R.R., Goldman, A., Jacquemart, D., Kleiner, I., Lacome, N., Lafferty, W.J., Mandin, J.Y., Massie, S.T., Mikhailenko, S.N., Miller, C.E., Moazzen-Ahmadi, N., Naumenko, O.V., Nikitin, A.V., Orphal, J., Perevalov, V.I., Perrin, A., Predoi-Cross, A., Rinsland, C.P., Rotger, M., Šimečková, M., Smith, M.A.H., Sung, K., Tashkun, S.A., Tennyson, J., Toth, R.A., Vandaele, A.C., Vander Auwera, J., 2005. The HITRAN 2008 molecular spectroscopic database. *J. Quant. Spectrosc. Radiat. Transf.* 96, 139–204.
- Runkle, B.R.K., Wille, C., Gažović, M., Wilmking, M., Kutzbach, L., 2014. The surface energy balance and its drivers in a boreal peatland fen of northwestern Russia. *J. Hydrol.* 511, 359–373.
- Schotanus, P., Nieuwstadt, F.T.M., de Bruin, H.A.R., 1983. Temperature measurement with a sonic anemometer and its application to heat and moisture fluxes. *Bound.-Layer Meteorol.* 26, 81–93.
- Seemanns, K.A., Anderson, M.C., Kustas, W.P., Gao, F., Alfieri, J.G., McKee, L., Prueger, J.H., Hain, C.R., Cammalleri, C., Yang, Y., Xia, T., Sanchez, L., Mar Alsina, M., Vélez, M., 2015. Monitoring daily evapotranspiration over two California vineyards using Landsat 8 in a multi-sensor data fusion approach. *Remote. Sens. Environ.*, <http://dx.doi.org/10.1016/j.rse.2015.10.025>.
- Serrano-Ortiz, P., Kowalski, A.S., Domingo, F., Ruiz, B., Alados-Arboledas, L., 2008. Consequences of uncertainties in CO₂ density for estimating net ecosystem CO₂ exchange by open-path eddy covariance. *Boundary-Layer Meteorol.* 126, 209–218.
- Starkenburg, D., Fochesatto, G.J., Cristobal, J., Prakash, A., Gens, R., Alfieri, J.G., Nagano, H., Harazono, Y., Iwata, H., Kane, D.L., 2015. Temperature regimes and turbulent heat fluxes across a heterogeneous canopy in an Alaskan boreal forest. *J. Geophys. Res. Atmos.* 120, 1–13.
- Ueyama, M., Hirata, R., Mano, M., Hamotani, K., Harazono, Y., Hirano, T., Miyata, A., Takagi, K., Takahashi, Y., 2012. Influences of various calculation options on heat, water and carbon fluxes determined by open- and closed-path eddy covariance methods. *Tellus* B 64 (8), 19048.
- Verma, M., Friedl, M.A., Richardson, A.D., Kiely, G., Cescatti, A., Law, B.E., Wohlfahrt, G., Gielen, B., Rouspard, O., Moors, E.J., Toscano, P., Vaccari, F.P., Gianelle, D., Bohrer, G., Varlagin, A., Buchmann, N., van Gorsel, E., Montagnani, L., Propastin, P., 2014. Remote sensing of annual terrestrial gross primary productivity from MODIS: an assessment using the FLUXNET La Thuile data set. *Biogeosciences* 11, 2185–2200.
- Waldo, S., Chi, J., Pressley, S., O'Keeffe, P., Pan, W.L., Brooks, E., Huggins, D., Stöckle, C., Lamb, B., 2016. Assessing carbon dynamics at high and low rainfall agricultural sites in the inland Pacific Northwest US using the eddy covariance method. *Agric. For. Meteorol.* 218–219, 25–36.
- Webb, E.K., Pearman, G.I., Leuning, R., 1980. Correction of flux measurements for density effects due to heat and water vapour transfer. *Q. J. R. Meteorol. Soc.* 106, 85–100.
- Welles, J.M., McDermitt, D.K., 2005. Measuring carbon dioxide in the atmosphere. In: Hatfield, J.L., Baker, J.M. (Eds.), *Micrometeorology in Agricultural Systems*, pp. 267–300.
- Wohlfahrt, G., Fenstermaker, L.F., Arnone, J.A., 2008. Large annual net ecosystem CO₂ uptake of a Mojave Desert ecosystem. *Glob. Change Biol.* 14, 1475–1487.
- Wyngaard, J.C., 1981. The effects of probe-induced flow distortion on atmospheric turbulence measurements. *J. Appl. Meteorol.* 20, 784–794.
- Wyngaard, J.C., 1988. The effects of probe-induced flow distortion on atmospheric turbulence measurements: extension to scalars. *J. Atmos. Sci.* 45, 3400–3412.
- Yuan, G., Zhang, P., Shao, M.A., Luo, Y., Zhu, X., 2014. Energy and water exchanges over a riparian Tamarix spp. stand in the lower Tarim River basin under a hyper-arid climate. *Agric. For. Meteorol.* 194, 144–154.